

# Benefits of a Geosynchronous Orbit (GEO) Observation Point for Orbit Determination

Ray Byrne, Michael Griesmeyer, Ron Schmidt, Jeff Shaddix, and Dave Bodette  
*Sandia National Laboratories*

## ABSTRACT

Determining orbits of unknown objects is a fundamental space situational awareness activity. The U.S. Space Surveillance Network (SSN) currently relies on ground-based radars, optical telescopes, and the Space Based Space Surveillance (SBSS) System. The SBSS system overcomes many of the pitfalls of optical ground-based systems like limited observation times (e.g. weather and time of day) and measurement uncertainty from atmospheric effects. However, the SBSS satellite is in a low earth orbit (630 km, sun synchronous), and must look “up” for GEO objects. This paper analyzes the potential benefits of a GEO observation point for performing metric observations that are combined with ground-based data. Several different scenarios are considered to quantify the reduction in orbit uncertainty from these types of observations. All results are derived using an Extended Kalman filter (EKF) to process the observations. Orbital uncertainties are expressed in terms of the error covariance.

## 1. INTRODUCTION

This paper analyzes the potential benefits of a GEO observation point for performing metric observations that are combined with ground-based data. Several different scenarios are considered to quantify the reduction in orbit uncertainty from these types of observations. The sensors considered include: earth-based angle-only, earth-based angle and range, and space-based angle-only. All results are derived using an Extended Kalman Filter (EKF) to process the observations. Orbital uncertainties are expressed in terms of the error covariance.

There are several common techniques for orbit estimation: linear least squares, nonlinear least squares, sequential-batch least squares, the Kalman filter, and the Extended Kalman filter [1]. We selected the Extended Kalman filter (EKF) approach to orbit estimation for several reasons. First, the equations of motion are nonlinear. In addition, previous research has shown that the EKF converges much faster than a least squares approach [1]. Examples of EKF’s applied to the orbit estimation problem are found in [1-7]. For the purposes of this analysis, we assume that an initial orbit estimation has been performed. We are most interested in the potential increase in accuracy that a geosynchronous observation point might provide. Section 2 provides an overview of the equations of motion employed in this analysis. Section 3 presents the Extended Kalman filter formulation. Simulation results are summarized in Section 4.

## 2. EQUATIONS OF MOTION

For this analysis we consider several types of sensors: earth-based angle-only, earth-based angle and range, and space-based angle-only. The same mathematical model, shown in Fig. 2.1, is used for each type of sensor [1]. All measurements are made in the local reference frame ( $\hat{u}, \hat{n}, \hat{e}$ ) of each sensor. Angle-only measurements estimate the azimuth and elevation to the target. Angle and range measurements combine azimuth, elevation, and the range to the target contained in the slant range vector  $\rho$ .  $\mathbf{R}$  is the radius vector locating the sensor with respect to earth-centered inertial (ECI) coordinates. For ground-based sensors, the length of  $\mathbf{R}$  is the radius of the earth. For space-based sensors, the length of  $\mathbf{R}$  is the distance from the center of the earth to the sensor. The right ascension and declination of the spacecraft are given by  $\alpha$  and  $\delta$ , while  $\theta$  is the sidereal time of the observer and  $\lambda$  is the latitude of the observer. The east longitude from the sensor to the spacecraft is  $\phi$ . The observation is given by

$$\rho = \mathbf{r} - \mathbf{R} \quad (1.1)$$

In the non-rotating equatorial inertial reference frame the spacecraft location is given by the vector  $\mathbf{r}$  with components  $x$ ,  $y$ , and  $z$ . The components of the vector  $\rho$  are given by

$$\boldsymbol{\rho} = \begin{bmatrix} x - \|\mathbf{R}\| \cos \lambda \cos \theta \\ y - \|\mathbf{R}\| \cos \lambda \sin \theta \\ z - \|\mathbf{R}\| \sin \lambda \end{bmatrix} \quad (1.2)$$

The conversion from the inertial to the sensor coordinate system ( $\hat{\mathbf{u}}, \hat{\mathbf{n}}, \hat{\mathbf{e}}$ ) is given by

$$\begin{bmatrix} \rho_u \\ \rho_e \\ \rho_n \end{bmatrix} = \begin{bmatrix} \cos \lambda & 0 & \sin \lambda \\ 0 & 1 & 0 \\ -\sin \lambda & 0 & \cos \lambda \end{bmatrix} \begin{bmatrix} \cos \theta & \sin \theta & 0 \\ -\sin \theta & \cos \theta & 0 \\ 0 & 0 & 1 \end{bmatrix} \boldsymbol{\rho} \quad (1.3)$$

For an angle and range sensor (e.g. a radar), the observation equations are given by

$$\|\boldsymbol{\rho}\| = (\rho_u^2 + \rho_e^2 + \rho_n^2)^{1/2} \quad (1.4)$$

$$\text{az} = \tan^{-1} \left( \frac{\rho_e}{\rho_n} \right), \text{ azimuth angle} \quad (1.5)$$

$$\text{el} = \sin^{-1} \left( \frac{\rho_u}{\|\boldsymbol{\rho}\|} \right), \text{ elevation angle} \quad (1.6)$$

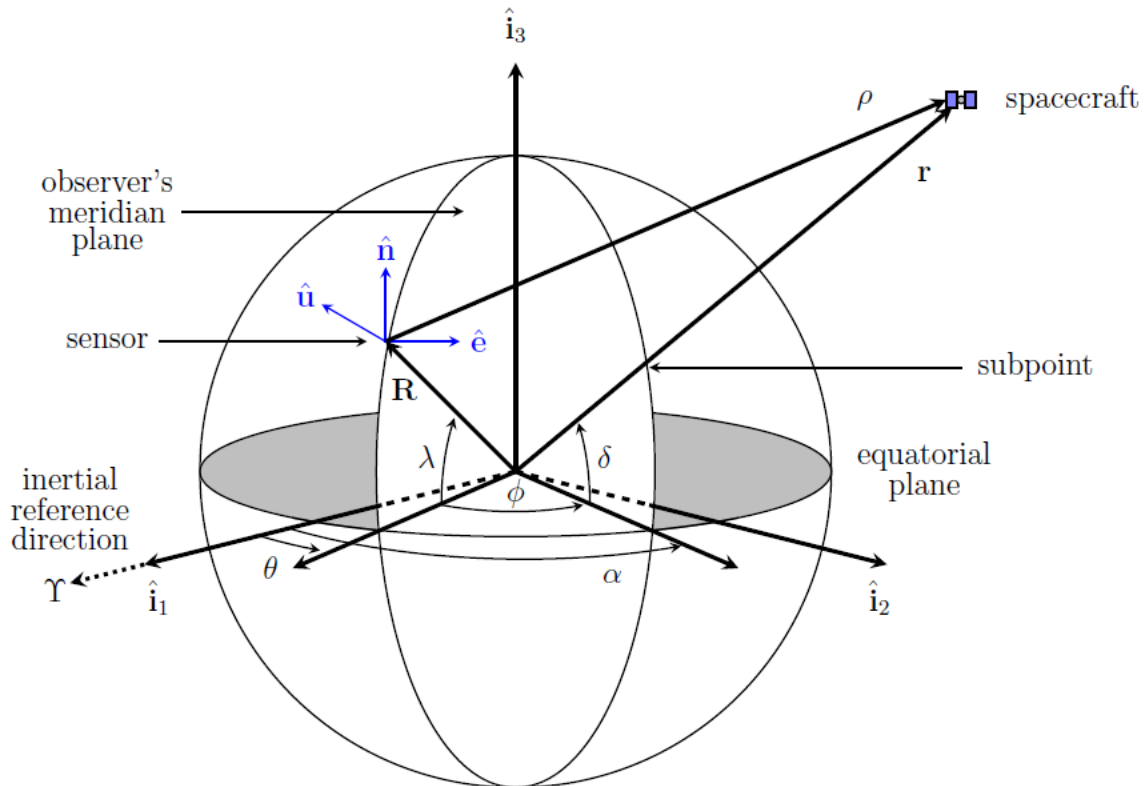


Fig. 2.1, Geometry of Sensor Observations [1]

The two-body orbital equations of motion are defined by [1]

$$\ddot{\mathbf{r}}(t) = -\frac{\mu}{\|\mathbf{r}(t)\|^3}\mathbf{r}(t) + \mathbf{w}(t) \quad (1.7)$$

where  $\mu$  is called the gravitation parameter

$$\mu \equiv \mathbf{GM} \quad (1.8)$$

$\mathbf{G}$  is the universal gravitation constant,  $\mathbf{M}$  is the mass of the earth, and  $\mathbf{w}(t)$  is the process noise. Examples of process noise include perturbing forces like thrusting, drag, solar pressure, and gravitational forces from other bodies (e.g. the sun and moon).

There are two approaches to solving the two-body orbital equations of motion. The first is to apply numerical integration techniques to equation (1.7). When other perturbations like drag are included, this is a reasonable approach. The second is to take advantage of the analytical solution for Keplerian motion. The six classical orbital elements are listed in Table 1 [2]. The transformations between the position/velocity state vector and the orbital elements are straightforward and described in [2, 8]. The orbital element reference frame,  $(\hat{P}, \hat{Q}, \hat{W})$ , and the definitions of  $\Omega$ ,  $\omega$  and  $i$  are defined in Figure 2.2.

Table 1, Classical Orbital Elements

Classical Orbital Element	Symbol
<b>semimajor axis:</b> defines the size of the elliptical orbit	$a$
<b>eccentricity:</b> defines the non-circularity of the orbit	$e$
<b>inclination:</b> defines the angle between the equatorial plane normal ( $\hat{K}$ ) and the orbital plane normal ( $\hat{W}$ )	$i$
<b>right ascension of the ascending node:</b> defines the angle between the vernal equinox direction ( $\hat{I}$ ) and the point where the satellite crosses the equatorial plane from the southern to northern hemisphere	$\Omega$
<b>argument of perigee:</b> defines the angle between the ascending node and the satellite's closest point of approach (perigee)	$\omega$
<b>true anomaly:</b> defines the angle between perigee and the satellite's actual position	$\nu$



$$\mathbf{x} = \begin{bmatrix} x \\ y \\ z \\ \dot{x} \\ \dot{y} \\ \dot{z} \end{bmatrix} \quad (1.12)$$

which contains the positions and velocities in the inertial reference frame. For a non-maneuvering object, there is no input  $\mathbf{u}(t)$  so the plant dynamics may be expressed as

$$\mathbf{f}(\mathbf{x}(t), t) = \begin{bmatrix} \dot{x} \\ \dot{y} \\ \dot{z} \\ -(\mu/r^3)x \\ -(\mu/r^3)y \\ -(\mu/r^3)z \end{bmatrix}, \quad r = \|\mathbf{r}\| \quad (1.13)$$

We have not included any perturbing forces for this analysis so  $G(t) = 0$  and  $Q(t) = 0(m, n)$ . The covariance matrix describing the uncertainty in the state estimate is  $P$ . The measured parameters  $\tilde{\mathbf{y}}_k$  are

$$\tilde{\mathbf{y}}_k = \begin{bmatrix} \|\rho\| \\ az \\ el \end{bmatrix}, \quad \text{angle/range measurement} \quad (1.14)$$

$$\tilde{\mathbf{y}}_k = \begin{bmatrix} az \\ el \end{bmatrix}, \quad \text{angle-only measurement} \quad (1.15)$$

The initialization step is

$$\hat{\mathbf{x}}(t_0) = \hat{\mathbf{x}}_0 \quad (1.16)$$

$$P_0 = E \left\{ \hat{\mathbf{x}}(t_0) \hat{\mathbf{x}}^T(t_0) \right\} \quad (1.17)$$

The Kalman filter gain step is

$$K_k = P_k^- H_k^T(\hat{\mathbf{x}}_k^-) [H_k(\hat{\mathbf{x}}_k^-) P_k^- H_k^T(\hat{\mathbf{x}}_k^-) + R_k]^{-1} \quad (1.18)$$

$$H_k(\hat{\mathbf{x}}_k^-) \equiv \left. \frac{\partial \mathbf{h}}{\partial \mathbf{x}} \right|_{\hat{\mathbf{x}}(t)} \quad (1.19)$$

For the range and angle measurement, we have

$$\frac{\partial \mathbf{h}}{\partial \mathbf{x}} = \begin{bmatrix} \frac{\partial \|\boldsymbol{\rho}\|}{\partial x} & \frac{\partial \|\boldsymbol{\rho}\|}{\partial y} & \frac{\partial \|\boldsymbol{\rho}\|}{\partial z} \\ \frac{\partial \text{az}}{\partial x} & \frac{\partial \text{az}}{\partial y} & \frac{\partial \text{az}}{\partial z} \\ \frac{\partial \text{el}}{\partial x} & \frac{\partial \text{el}}{\partial y} & \frac{\partial \text{el}}{\partial z} \end{bmatrix} \quad (1.20)$$

From [1],

$$\frac{\partial \|\boldsymbol{\rho}\|}{\partial x} = (\rho_u \cos \lambda \cos \theta - \rho_e \sin \theta - \rho_n \sin \lambda \cos \theta) / \|\boldsymbol{\rho}\| \quad (1.21)$$

$$\frac{\partial \|\boldsymbol{\rho}\|}{\partial y} = (\rho_u \cos \lambda \sin \theta - \rho_e \cos \theta - \rho_n \sin \lambda \sin \theta) / \|\boldsymbol{\rho}\| \quad (1.22)$$

$$\frac{\partial \|\boldsymbol{\rho}\|}{\partial z} = (\rho_u \sin \lambda - \rho_n \cos \lambda) / \|\boldsymbol{\rho}\| \quad (1.23)$$

$$\frac{\partial \text{az}}{\partial x} = \frac{1}{(\rho_n^2 + \rho_e^2)} (\rho_e \sin \lambda \cos \theta - \rho_n \sin \theta) \quad (1.24)$$

$$\frac{\partial \text{az}}{\partial y} = \frac{1}{(\rho_n^2 + \rho_e^2)} (\rho_e \sin \lambda \sin \theta - \rho_n \cos \theta) \quad (1.25)$$

$$\frac{\partial \text{az}}{\partial z} = \frac{1}{(\rho_n^2 + \rho_e^2)} \rho_e \cos \lambda \quad (1.26)$$

$$\frac{\partial \text{el}}{\partial x} = \frac{1}{\|\boldsymbol{\rho}\|(\|\boldsymbol{\rho}\|^2 - \rho_u^2)^{1/2}} \left( \|\boldsymbol{\rho}\| \cos \lambda \cos \theta - \rho_u \frac{\partial \|\boldsymbol{\rho}\|}{\partial x} \right) \quad (1.27)$$

$$\frac{\partial \text{el}}{\partial y} = \frac{1}{\|\boldsymbol{\rho}\|(\|\boldsymbol{\rho}\|^2 - \rho_u^2)^{1/2}} \left( \|\boldsymbol{\rho}\| \cos \lambda \sin \theta - \rho_u \frac{\partial \|\boldsymbol{\rho}\|}{\partial y} \right) \quad (1.28)$$

$$\frac{\partial \text{el}}{\partial z} = \frac{1}{\|\boldsymbol{\rho}\|(\|\boldsymbol{\rho}\|^2 - \rho_u^2)^{1/2}} \left( \|\boldsymbol{\rho}\| \sin \lambda - \rho_u \frac{\partial \|\boldsymbol{\rho}\|}{\partial z} \right) \quad (1.29)$$

For angle-only measurements, we have

$$\frac{\partial \mathbf{h}}{\partial \mathbf{x}} = \begin{bmatrix} \frac{\partial \text{az}}{\partial x} & \frac{\partial \text{az}}{\partial y} & \frac{\partial \text{az}}{\partial z} \\ \frac{\partial \text{el}}{\partial x} & \frac{\partial \text{el}}{\partial y} & \frac{\partial \text{el}}{\partial z} \end{bmatrix} \quad (1.30)$$

The Kalman filter update step is given by

$$\hat{\mathbf{x}}_k^+ = \hat{\mathbf{x}}_k^- + K_k [\hat{\mathbf{y}}_k - \mathbf{h}(\hat{\mathbf{x}}_k^-)] \quad (1.31)$$

$$P_k^+ = [I - K_k H_k(\hat{\mathbf{x}}_k^-)] P_k^- \quad (1.32)$$

Since  $G(t) = 0$ , the propagation step is given by

$$\dot{\hat{\mathbf{x}}} = \mathbf{f}(\hat{\mathbf{x}}(t), t) \quad (1.33)$$

$$P_{k+1}^- = \Phi_k P_k^+ \Phi_k^T \quad (1.34)$$

where  $\Phi_k$  is the discrete-time representation of the  $F$  matrix defined by

$$\Phi_k = e^{F\Delta t}, \quad F = \begin{bmatrix} 0_{3 \times 3} & I_{3 \times 3} \\ F_{21} & 0_{3 \times 3} \end{bmatrix} \quad (1.35)$$

with

$$F_{21} = \begin{bmatrix} \frac{3\mu x^2}{\|\mathbf{r}\|^5} - \frac{\mu}{\|\mathbf{r}\|^3} & \frac{3\mu xy}{\|\mathbf{r}\|^5} & \frac{3\mu xz}{\|\mathbf{r}\|^5} \\ \frac{3\mu xy}{\|\mathbf{r}\|^5} & \frac{3\mu y^2}{\|\mathbf{r}\|^5} - \frac{\mu}{\|\mathbf{r}\|^3} & \frac{3\mu yz}{\|\mathbf{r}\|^5} \\ \frac{3\mu xz}{\|\mathbf{r}\|^5} & \frac{3\mu yz}{\|\mathbf{r}\|^5} & \frac{3\mu z^2}{\|\mathbf{r}\|^5} - \frac{\mu}{\|\mathbf{r}\|^3} \end{bmatrix} \quad (1.36)$$

Details on calculating  $\Phi_k$  via a series expansion can be found in [1].

#### 4. SIMULATION RESULTS

In order to quantify the potential benefits of a geostationary observation point for improving the accuracy of metric observations, the following five scenarios were considered:

- Ground-based angle-only sensors
- Ground-based angle-only and angle/range sensors
- Ground-based angle-only and space-based angle-only sensors
- Ground-based angle/range and space-based angle-only sensors
- Ground-based angle-only, angle/range and space-based angle-only sensors

A simulated geosynchronous satellite, based on the TDRS (Tracking and Data Relay Satellite) 8 orbit with nodal position of -46.67 degrees longitude, was used as the object of interest. An extended Kalman Filter was used to estimate its state. Monte Carlo simulations were employed to quantify the expected performance of all scenarios. Quantities varied over the Monte Carlo simulations include: initial orbit uncertainty, sensor location, and sensor noise. For the first study a set of Monte Carlo runs with the parameters in Table 2 were used. The results are summarized in Table 3. The location of the sensor relative to the satellite track is illustrated in Figure 4.1. The noise parameters for the different sensors were based on the representative calibration values presented in [2].

## Satellite Trajectory and Observations

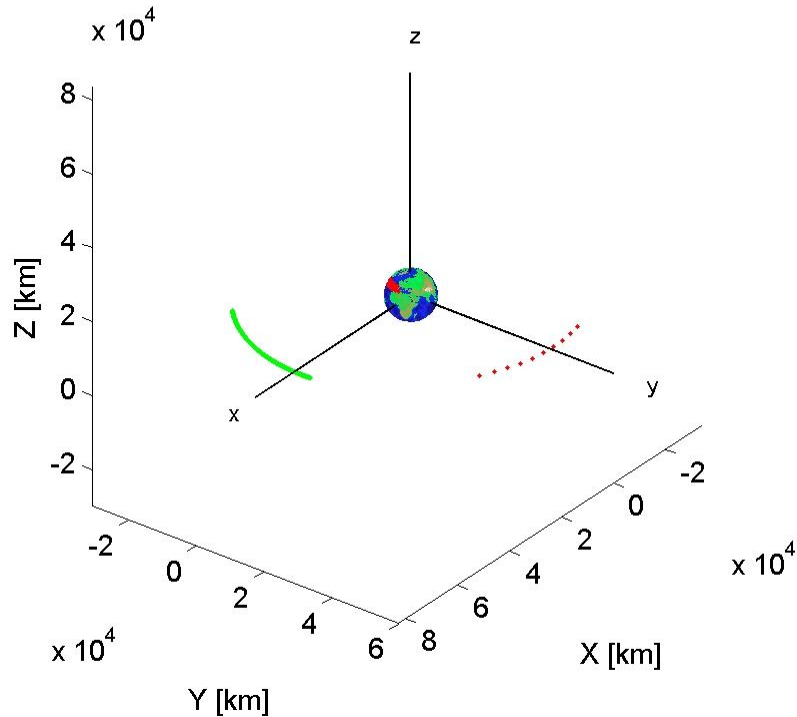


Figure 4.1, Sensor-Satellite Configuration (green line is the satellite track, the red dots represent the sensor locations when a measurement is taken).

Table 2, Configuration for First Study

Number of Monte Carlo Runs	100
Nodal position of geostationary target	-46.67 degrees
Latitude of angle-only earth sensor	33.82 degrees
Latitude of angle-range and second angle-only earth sensor	42.62 degrees
Longitude of earth sensors	Centered at target nodal position separated by a randomly selected angle between 0 and 20 degrees
Nodal position geostationary space based sensor	Target node + 120 degrees plus a randomly selected offset between -10 and +10 degrees
Angle-only earth sensor noise $\sigma$	0.003 degrees
Angle-range earth sensor angle noise $\sigma$	0.01 degrees
Angle-range earth sensor range noise $\sigma$	0.15 km
Angle-only space based sensor noise $\sigma$	0.003 degrees
Initial position error $\sigma$	20.0 km
Initial velocity error $\sigma$	0.05 times initial velocity (5 percent of the initial velocity)

The roughly 14 km position error for the ground based angle-only sensors case was much larger than the other cases because the angle between the sensors was small and provided little resolution in the X direction. The case with ground and spaced-based angle only sensors did much better because the angle between the measurements was large enough to provide good triangulation for the satellite position. The cases with the angle/range sensor and one angle

only sensor are better because the range estimate from this sensor is very good (~.15 km) and is able to significantly reduce the X coordinate error.

Table 3, Summary of First Study Monte Carlo Simulation Results

Parameter	Gnd angle-only, Gnd angle-only	Gnd angle-only, Gnd angle/range	Gnd angle-only, Space angle-only	Gnd angle/range, Space angle-only	Gnd angle-only, Gnd angle/range, Space angle-only
Mean RMS Position Error $\sigma$	13.829 km	1.347 km	4.494 km	1.676 km	1.039 km
Mean X Position Error $\sigma$	13.627 km	0.262 km	4.196 km	0.274. km	0.215 km
Mean Y Position Error $\sigma$	1.071 km	0.558 km	1.270 km	1.152 km	0.540 km
Mean Z Position Error $\sigma$	2.078 km	1.198 km	0.968 km	1.183 km	0.861 km
Mean RMS Velocity Error $\sigma$	1.348 m/s	0.167 m/s	0.602 m/s	0.182 m/s	0.127 m/s
Mean X Velocity Error $\sigma$	1.194 m/s	0.051 m/s	0.534. m/s	0.089 m/s	0.046 m/s
Mean Y Velocity Error $\sigma$	0.610 m/s	0.048 m/s	0.250 m/s	0.054 m/s	0.047 m/s
Mean Z Velocity Error $\sigma$	0.135 m/s	0.151 m/s	0.120 m/s	0.149 m/s	0.109 m/s

A second study was performed to explore the effect of angular error variations for spaced-based angle-only sensors. Cases were run for the space based sensor with angle noise increased by a factor of five (0.015 degrees) and decreased by a factor of five (0.0006 degrees). The results are shown in Table 4. Results for the case with earth angle-only earth angle/range sensors and space based angle-only sensor with noise of 0.015 degrees are not in the table because they were within 2% of the results for the earth angle-only earth angle/range sensors by themselves. Comparing Table 4 with Table 3, it is seen that the space based angle only sensor with 0.015 degrees noise is still slightly better than the earth based angle-only sensor when paired with either of the ground based sensors. The decreased noise version of the space based sensor when paired with the angle-only earth sensor does about a factor of two better than the nominal noise spaced-based sensor. When paired with the angle-range earth sensor it does about factor of three better than the nominal noise of a spaced-based sensor.

Table 4, Summary of Second Study Monte Carlo Simulation Results

Parameter	Gnd angle-only, Space angle-only 0.015 degrees	Gnd angle/range, Space angle-only 0.015 degrees	Gnd angle-only, Space angle-only 0.0006 degrees	Gnd angle/range, Space angle-only 0.0006 degrees	Both Gnd, Space angle-only 0.0006 degrees
Mean RMS Position Error $\sigma$	12.289 km	3.932 km	1.948 km	0.511 km	0.468. km
Mean X Position Error $\sigma$	12.039 km	0.653 km	1.630 km	0.146 km	0.141 km
Mean Y Position Error $\sigma$	1.419 km	1.705 km	1.023 km	0.422 km	0.376 km
Mean Z Position Error $\sigma$	2.001 km	3.482 km	0.264 km	0.247 km	0.238 km
Mean RMS Velocity Error $\sigma$	1.271 m/s	0.466 m/s	0.266 m/s	0.062 m/s	0.058 m/s
Mean X Velocity Error $\sigma$	1.133 m/s	0.151 m/s	0.217 m/s	0.033 m/s	0.030 m/s
Mean Y Velocity Error $\sigma$	0.544 m/s	0.061 m/s	0.148 m/s	0.042 m/s	0.039 m/s
Mean Z Velocity Error $\sigma$	0.180 m/s	0.437 m/s	0.034 m/s	0.031 m/s	0.030 m/s

## 5. SUMMARY AND CONCLUSIONS

In this paper we have compared the expected orbit estimation uncertainty for several different sensor configurations. The contribution of a spaced-based angle-only sensor in geostationary orbit to the determination of the orbit of another geostationary satellite was explored. Pairing an earth-based angle-only sensor has advantages over pairing two earth-based angle-only sensors because the angle between the target and the spaced-based and earth based sensor is much larger than is achievable than that for two earth-based sensor. The advantage remains even if the noise for space-based sensor is a factor of five greater than that for the earth-based sensor. When the geosynchronous spaced-based sensor noise is a factor five lower than that for the earth-based sensor, the spaced-based sensor and the earth-based angle-range sensor alone are a factor of two better than the earth-based angle-only, earth-based angle-range and spaced-based sensors all with nominal noise. Thus, for the scenario considered, it is clearly beneficial to combine information from a geosynchronous observation point when estimating the orbit of another geosynchronous object. Although there are an infinite number of possible scenarios, these preliminary results indicate that a geosynchronous observation point provides a quantifiable benefit for estimating the orbits of other geosynchronous objects.

## 6. ACKNOWLEDGEMENTS

This work was funded by the Operationally Responsive Space office in Albuquerque New Mexico. The MATLAB<sup>®</sup> code provided as a supplement to *Optimal Estimation of Dynamic Systems* [1] was used as a starting point for the simulations performed under this effort. The results were confirmed with C++ code developed independently by Michael Griesmeyer.

## 7. REFERENCES

1. John L. Crassidis and John L. Junkins, *Optimal Estimation of Dynamic Systems*, Chapman & Hall/CRC, Boca Raton, Florida, 2004.
2. David. A. Vallado, *Fundamentals of Astrodynamics and Applications*, Microcosm Press, El Segundo, California, 2<sup>nd</sup> Edition, 2004.
3. Bryon D. Tapley, Bob E. Schutz, and George H. Born, *Statistical Orbit Determination*, Elsevier Academic Press, Burlington, Massachusetts, 2004.
4. Bruno O.S. Teixeira, Mario A. Santillo, R. Scott Erwin, and Dennis S. Bernstein, "Spacecraft tracking using sampled-data Kalman filters," *IEEE Control Systems Magazine*, pp. 78-94, August 2008.
5. Daniel J. Brett, "Orbital estimation using an extended Kalman filter," Ph.D. Dissertation, Naval Postgraduate School, Monterey, California, December 1992.
6. D.A. Cicci and G.H. Ballard, "Sensitivity of an extended Kalman filter 1. variation in the number of observers and types of observations," *Appl. Math. Comput.*, vol. 66, pp. 233–246, 1994.
7. D.A. Cicci and G.H. Ballard, "Sensitivity of an extended Kalman filter 2. variation in the observation error levels, observation rates, and types of observations," *Appl. Math. Comput.*, vol. 66, pp. 247–259, 1994.
8. Howard A. Curtis, *Orbital Mechanics for Engineering Students*, Butterworth-Heinemann/Elsevier Ltd., Burlington, Massachusetts, 2<sup>nd</sup> Edition, 2010.